GAS-SURFACE INTERACTION EFFECTS ON FLOWFIELD STRUCTURE OF A REENTRY BRAZILIAN CAPSULE

Wilson F. N. Santos wilson@lcp.inpe.br
Combustion and Propulsion Laboratory (LCP)
National Institute for Space Research (INPE)
Cachoeira Paulista-SP, 12630-000, BRAZIL

Abstract. *A numerical study has been conducted to assess the effects of the gas-surface interaction on the flowfield structure of the Brazilian capsule SARA (acronym for SAtélite de Reentrada Atmosférica) reentering from Low Earth Orbit. Effects of incomplete surface accommodation on the vehicle flowfield structure are highlighted. Several numerical results, between full and incomplete surface accommodation coefficients, are provided and compared to establish the model influence on the primary properties, such as velocity, density, pressure, and temperature adjacent to the vehicle surface. Seven combinations of normal and tangential accommodation coefficients associated to five different altitudes were used in the simulation. These parameters are of primary relevance for the design of the reentry trajectory and the vehicle thermal protection system. The numerical study employed the Direct Simulation Monte Carlo (DSMC) method in conjunction with the Cercignani-Lampis-Lord gas surface interaction model. Results substantiate that it becomes imperative to take surface accommodation into account in order to make accurate predictions of the aerothermodynamic aspects of the capsule at hypersonic flow.*

Keywords: *DSMC, Hypersonic flow, Rarefied flow, Reentry capsule, SARA.*

1 INTRODUCTION

Nowadays, one of the major programs of the Brazilian Program for Space Activities, officially called PNAE (acronym for Programa Nacional de Atividades Espaciais), is related to a reusable orbital platform, named SARA (acronym for SAtélite de Reentrada Atmosférica), for scientific and technological experiments in low gravity environment. The system, build in a platform with a capsule shape, will stay in orbit during the time needed for the execution of the experiments, being sent back to the Earth, and then recovered. The development of reusable space vehicles (capsules) for experiments in a microgravity environment has lately drawn considerable interest in the aerothermodynamics of these vehicles along the entire flight trajectory.

The correct prediction of the aerothermodynamics aspects of reentry vehicles along their entire trajectory is often an important step in their design phase. In the Earth atmosphere reentry, vehicles undergo not only different velocity regimes – hypersonic, supersonic and subsonic – but also different flow regimes – free molecular flow, transition and continuum – and flight conditions that may difficult their aerodynamic design. In the molecular flow or in the transition flow regime, which can characterize a large portion of the reentry path, hypersonic vehicles may encounter non-equilibrium conditions that can have a significant influence on the aerodynamic performance. In this fashion, the assessment of aerodynamic forces and heat fluxes in these regimes are very important for planning the reentry mission.

Certainly, an understanding of flow phenomena in non-equilibrium conditions can be gained by flight testing and wind-tunnel testing. Nevertheless, both testings are expensive and danger. These factors are mitigated by computer simulations, although computer simulations can not eliminate physical experimentation. However, they can greatly reduce the amount of such experimentation. In addition, numerical techniques, which fail to incorporate non-equilibrium conditions, miss out on an essential part of the flow physics surrounding the reentry vehicle.

According to the current literature, for the particular case of SARA capsule, only a few studies (Toro $et\ al.$, 2001; Sharipov, 2003; Toro $et\ al.$, 2004; Pimentel $et\ al.$, 2005; Tchuen $et\ al.$, 2005; Kozak and Sharipov, 2012; Santos, 2012) has been dedicated to investigate the aerothermodynamics of the capsule reentering the Earth atmosphere. For the purpose of this introduction, it will be sufficient to describe only some of these studies.

Pimentel $et\ al.$ (2005) have performed inviscid hypersonic flow simulations over the SARA capsule by employing the planar two-dimensional (2-D) and the axisymmetric Euler equations. Results were presented for an altitude of 80 km, Mach numbers of 15 and 18, and angle of attack of 0 and 10 degrees. They also considered air as the working fluid composed of five species (N_2, O_2, O, N, and NO) with their reactions of dissociation and recombination. Pressure and temperature contour maps were presented for 2-D and axisymmetric flow.

Tchuen $et\ al.$ (2005) have investigated the flowfield structure over the SARA capsule by using axisymmetric Navier-Stokes equations. The analysis considered hypersonic flow at zero angle of attack in chemical and thermal non-equilibrium. It was assumed air as the working fluid composed of seven species (N_2, O_2, O, N, NO, NO^+, and e^-) associated with their reactions of dissociation and recombination. Results for pressure, skin friction, and heat transfer coefficients were presented

for different combinations of Mach numbers of 10, 20 and 25 with altitudes of 75 km and 80 km.

Finally, Santos (2012) has investigated the flowfield structure of a hypersonic flow over the SARA capsule in the reentry trajectory, from 100 km to 80 km, by employing the DSMC method. This range basically covered the transition flow regime, i.e., between the free collision flow and the continuum flow regime. The primary goal was to assess the sensitivity of the primary properties, velocity, density, pressure, and temperature due to changes on the altitude representative of a typically reentry trajectory of the SARA capsule. The investigation considered two species (N_2 and O_2) as the working fluid, and rotation and vibration internal modes of energy.

The previous work (Santos, 2012) on hypersonic flow past SARA capsule has concentrated primarily on the analysis of the flowfield structure by considering the diffuse reflection model as being the gas-surface interaction. The diffuse model assumes that the molecules are reflected equally in all directions, quite independently of their incident speed and direction. Nevertheless, as a space flight vehicle is exposed to a rarefied environment over a considerable time, a departure from the fully diffuse model is observed, resulting from colliding molecules that clean the surface of the vehicle, which becomes gradually decontaminated. Molecules reflected from clean surfaces show lobular distribution in direction. The flux distribution of scattered molecules emitted from clean surfaces frequently has a lobular shape that is centered about an angle, which tends to approach the specular angle for very high energies and/or low angle of attack (Bird, 1994).

In this framework, the present account extends the previous analysis (Santos, 2012) by examining the gas-surface interaction impact on the flowfield structure around the SARA capsule for the same reentry conditions. In this fashion, the primary goal of this study is to assess the sensitivity of the primary properties, such as velocity, density, pressure, and temperature, due to variations in the surface accommodation coefficients by employing the Cercignani-Lampis-Lord (CLL) model (Lord, 1991). The CLL model, which incorporates independent accommodation coefficients for the normal and tangential momentum components of reflected molecules, is implemented into the DSMC code, and simulations are performed by assuming the axisymmetric hypersonic flow over the SARA capsule.

2 GAS-SURFACE INTERACTION MODEL

The essential phenomena of rarefied gases are found mostly in the region relatively near to the solid boundaries, i.e., within a few mean free paths. A knowledge of the physics of the interaction of gas molecules and solid surfaces is thus of primary importance. In hypersonic flight at high altitudes, gas-surface interaction is the dominant physical process governing aerodynamic forces and heat transfer. Both the aerodynamic surface quantities and the state of the gas adjacent to the body surface are very sensitive to the assumptions used in the calculation concerning the gas-surface interaction model for transition and free molecular flows.

As the majority of the practical engineering problems involves gas-surface interaction phenomena, a suitable boundary condition is required in order to obtain reliable results from numerical simulation of rarefied gas flows. Three models of gas-surface interactions may be employed in the DSMC method as practical models for purpose of engineering surfaces: (1) specular reflection,

(2) diffuse reflection, and (3) some combination of these. In a specular reflection, molecules are reflected like a perfectly elastic sphere with reversal of the normal component of velocity and no change in the parallel component of velocities and energy. In a diffuse reflection, the molecules are reflected equally in all directions usually with a complete thermal accommodation. The final velocity of the molecules is randomly assigned according to a half-range Maxwellian distribution determined by the wall temperature. The combination of diffuse reflection with specular reflection, known as Maxwell model (Maxwell, 1879), introduces a single parameter f to indicate the fraction of those molecules reflected diffusely in a completely accommodated fashion according to a Maxwellian distribution corresponding to the wall temperature, and the remaining fraction $(1-f)$, being assumed to reflect specularly. Usually, the parameter f in the Maxwell model is identified by the tangential accommodation coefficient σ_t.

The popularity of the Maxwell model (Maxwell, 1879) is explained apparently by its simplicity and by the fact that it satisfies reciprocity, i.e., the principle of detailed balance. Nevertheless, the Maxwell model does not accurately describe the detailed molecular behavior observed in fundamental gas-surface scattering experiments under certain conditions. A phenomenological model that also satisfies the reciprocity conditions and has demonstrated improvement over the Maxwell model has been proposed by Cercignani and Lampis (1971), known as CL model. This model is based on the definition of two parameters α_n and σ_t that represent the accommodation coefficient for the kinetic energy associated with the normal component of velocity, and the parallel momentum accommodation, respectively. They are given by the following equations,

$$\alpha_n = \frac{e_i - e_r}{e_i - e_w} \tag{1}$$

$$\sigma_t = \frac{\tau_i - \tau_r}{\tau_i} \tag{2}$$

where e and τ refer to the average kinetic energy for the normal component of velocity, and momentum flux acting tangential to the surface, respectively; subscripts i and r stand for the incident and reflected components, and w refers to the component that would be produced by a diffuse reflection at the surface temperature.

The CL model provides a continuous spectrum of behavior from specular reflection at one end to diffuse reflection with complete energy accommodation at the other, and produces physically realistic distributions of direction and energy re-emitted molecules.

The probability distribution function for the component of velocity normal to the surface is given by,

$$P_n(v_n'|v_n) = \frac{2v_n'}{\alpha_n} I_0(2\sqrt{1-\alpha_n}\frac{v_n v_n'}{\alpha_n}) \exp[-\frac{v_n'^2 + (1-\alpha_n)v_n^2}{\alpha_n}] \tag{3}$$

where I_0 is the modified Bessel function, v_n' and v_n are the incident and reflect velocity components normalized by the most probable molecular speed at the surface temperature, and defined by

$\sqrt{2kT_w/m}$.

The probability distribution function for the component of velocity parallel to the surface is given by,

$$P_t(\mathbf{v}'_t|\mathbf{v}_t) = \frac{1}{\sqrt{\pi\sigma_t(2-\sigma_t)}} \exp\{-\frac{v'_t - (1-\sigma_t)v_t]^2}{\pi\sigma_t(2-\sigma_t)}\} \tag{4}$$

where $\mathbf{v}'_t$ and $\mathbf{v}_t$ are the incident and reflect tangential velocity vector also normalized by the most probable molecular speed at the surface temperature.

Lord (1991) has implemented the CL model into the DSMC method, and presented a simple method for generating random sample velocities from Eqs. (3) and (4). The DSMC method with Lord's implementation is referred as the Cercignani-Lampis-Lord (CLL) model. For comparison purpose, Fig. 1 displays a schematic drawing representing the Maxwell reflection model and the CLL reflection model.

It should be emphasized the CLL model was derived by assuming that there is no coupling between the normal and tangential momentum components. The two adjustable parameters appearing in the CLL model are the normal component of translational energy α_n and the tangential component of momentum σ_t. However, in the implementation of the CLL model in the DSMC method, Bird (1994) has shown that it is equivalent to specify the normal α_n and tangential α_t components of translational energy, since $\alpha_t = \sigma_t(2-\sigma_t)$, and thus that $\sigma_t < \alpha_t$, by assuming that σ_t lies between 0 and 1. In the present account, α_n and σ_t are used as being the two adjustable parameters.

Finally, it should be mentioned in this context that many studies have been made using both the CL and the CLL models to analyze the behavior of molecules reflected from surface. Of particular interest are the application of the CL model described in Cercignani (1972) and those on CLL model discussed by Woronowicz and Rault (1994) and Hedahl and Wilmoth (1995).

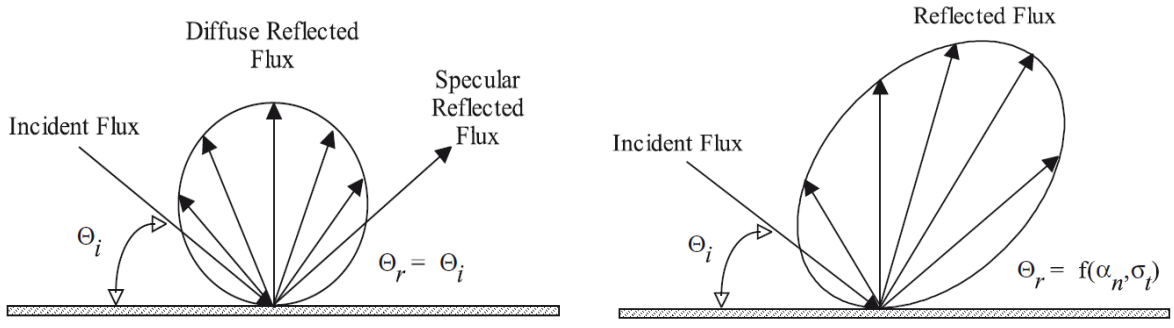

(a) **Maxwell Model** (b) **CLL Model**

Figure 1: Drawing illustrating the Maxwell reflection model and the CLL reflection model.

3 COMPUTATIONAL TOOL

In the analysis of aerothermodynamic characteristics of aerospace vehicles, along their descending flight trajectory through the Earth atmosphere, different computational methods are required. At high altitudes, the aerothermodynamic predictions are related to the free molecular or to transition flow regime. In these flow regimes, where physical phenomena with a significant degree of non-equilibrium are present, the Direct Simulation Monte Carlo (DSMC) method is usually employed. The applicability of DSMC method covers from the free molecular regime to the near-continuum regime where it overlaps with that of the continuum approaches. At low altitudes, the aerothermodynamic predictions are related to the continuum flow regime. In this regime, computational methods such as Computational Fluid Dynamics (CFD) are employed. In the present account, the vehicle is subjected to the conditions characterized by the transition flow regime. In this fashion, DSMC method is the suitable computational tool in order to investigate the gas-surface interactions.

The DSMC method, pioneered by Bird (1994), has become the most common computational technique for modeling complex transitional flows of engineering interest. In the DSMC method, the gas flow is represented by a defined number of simulated particles, where each simulated particle represents a large number of real gas particles. The simulated particles are allowed to move, to collide among themselves, and with the boundaries of the domain, while the computer stores their position coordinates, velocities and other physical properties, such as internal energy.

The DSMC algorithm consists of four primary processes: (1) move the particles, (2) index and cross reference the particles, (3) simulate collisions, and (4) sample the flowfield. The molecular movement process is modeled deterministically. Molecules are allowed to move along their trajectory over a time interval for a distance that depends on their speed. The time interval should be less than the mean time between intermolecular collisions (Bird, 1994). During the movement process, a molecule can stay inside the same cell, move to another adjacent cell, reflect from the wall boundary or leave the computational domain at the outflow boundary. The second process is related to indexing and tracking the molecules. This process is a prerequisite for the two other processes, i.e., molecular collisions and sampling the flowfield. Accurate and fast indexing and tracking are key issues in DSMC applications related to a large-scale processing. The next process takes into account the particle-particle interactions. The particle-to-particle collisions are treated in a probabilistic base. Finally, the macroscopic properties are sampled from simple weighting averages of microscopic properties.

Collisions in the present DSMC code are modeled by using the variable hard sphere (VHS) molecular model (Bird, 1981) and the no time counter (NTC) collision sampling technique (Bird, 1989). Repartition energy among internal and translational modes is controlled by the Larsen-Borgnakke statistical model (Borgnakke and Larsen, 1975). Simulations are performed using a non-reacting gas model for a constant freestream gas composition consisting of 76.3% of N_2 and 23.7% of O_2. Energy exchanges between the translational and internal modes, rotational and vibrational, are considered. The probability of an inelastic collision determines the rate at which energy is transferred between the translational and internal modes after an inelastic collision. For a given collision, the probability is defined by the inverse of the number of relaxation, $1/Z_R$ for rotation

and $1/Z_V$ for vibration, where Z_R and Z_V correspond to the number of collisions needed, on average, for a molecule to undergo relaxation. In the present account, relaxation collision numbers of 5 and 50 were used for the calculations of rotation and vibration, respectively.

4 GEOMETRY DEFINITION

In the present account, the SARA capsule geometry follows that one defined in the previous study (Santos, 2012). The capsule is an axisymmetric design consisting of a spherical nose with a 11.4-degree half-angle conical afterbody. The nose radius R is 0.2678 m, the afterbody base has a radius R_B of 0.5035 m, and the total length L is 1.410 m. Figure 2(a) illustrates schematically the capsule shape and the main important physical and geometric parameters related to the hypersonic flow on the capsule. The main physical parameters are defined as follows: M_∞ is the freestream Mach number, Kn_∞ stands for the Knudsen number, T_w is the wall temperature, and finally, α_n and σ_t are the accommodation coefficients.

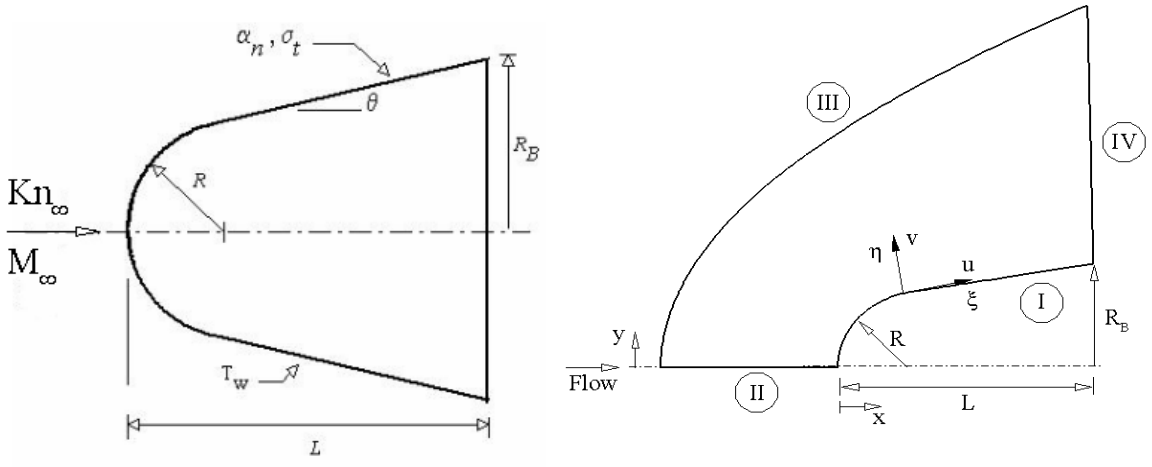

(a) (b)

Figure 2: Drawing illustrating (a) a schematic view of the capsule and (b) the computational domain.

5 FREESTREAM AND FLOW CONDITIONS

Freestream flow conditions are those given in the previous investigation (Santos, 2012) and summarized in Table 1, and the gas properties (Bird, 1994) are tabulated in Table 2. Based on this set of tables, T_∞, p_∞, ρ_∞, n_∞, λ_∞, and V_∞ represent, respectively, temperature, pressure, density, number density, molecular mean free path, and velocity. In addition, χ, m, d and ω stand respectively for mass fraction, molecular mass, molecular diameter and viscosity index.

Table 1: Freestream flow conditions (Santos, 2012).

Altitude (km)	T_∞(K)	p_∞(N/m^2)	ρ_∞(kg/m^3)	n_∞(m^{-3})	λ_∞(m)	V_∞(m/s)
80	180.7	1.03659	1.999×10^{-5}	4.1562×10^{21}	3.085×10^{-3}	7820
85	180.7	0.41249	7.956×10^{-6}	1.6539×10^{20}	7.751×10^{-3}	7864
90	180.7	0.16438	3.171×10^{-6}	6.5908×10^{19}	1.945×10^{-2}	7864
95	195.5	0.06801	1.212×10^{-6}	2.5197×10^{19}	5.088×10^{-2}	7866
100	210.0	0.03007	4.989×10^{-7}	1.0372×10^{19}	1.236×10^{-1}	7862

Table 2: Gas properties (Bird, 1994).

	χ	m (kg)	d (m)	ω
O_2	0.237	5.312×10^{-26}	4.01×10^{-10}	0.77
N_2	0.763	4.650×10^{-26}	4.11×10^{-10}	0.74

The freestream velocity V_∞ of 7862, 7866, 7864, 7864, and 7820 m/s, for altitude of 100, 95, 90, 85, and 80 km is based on the velocity-altitude map for the SARA capsule (Santos, 2012). In addition, these values correspond to a freestream Mach number M_∞ of 27.1, 28.1, 29.2, 29.2, and 29.0, respectively.

For the altitudes investigated, 100, 95, 90, 85, and 80 km, the overall Knudsen number, defined as the ratio of the freestream molecular mean free path λ_∞ to the nose radius R, corresponds to Kn_∞ of 0.4615, 0.1899, 0.0726, 0.0289, and 0.0115, respectively. The Reynolds number Re_∞ correspond to 92, 224, 609, 3442 and 15249 for altitudes of 100, 95, 90, 85 and 80 km, respectively, based on conditions in the undisturbed stream with the nose radius R as the characteristic length. Finally, the capsule surface was kept at a constant wall temperature T_w of 800 K for all cases investigated.

In order to simulate the incomplete surface accommodation, the CLL model implemented into the DSMC code considered only the normal and tangential accommodation coefficients. The internal energy accommodation was kept equal to one for all calculations presented in this work. Hence, α_n and σ_t are used as being the two adjustable parameters. The DSMC calculations were performed independently for four distinct numerical values for α_n and σ_t: 0.25, 0.50, 0.75, and 1. Therefore, when α_n is equal to 0.25, 0.50 or 0.75, σ_t is set equal to 1, and vice-versa. It is important to mention that $\alpha_n = 1 = \sigma_t$ represents the diffuse reflection case.

6 COMPUTATIONAL FLOW DOMAIN AND GRID

A schematic view of the computational domain is demonstrated in Fig. 2(b). Advantage of the flow symmetry is taken into account, and molecular simulation is applied to one-half of a full configuration. The computational domain used for the calculation is made large enough so that the capsule disturbances do not reach the upstream and side boundaries, where freestream conditions

are specified. In this fashion, the computational domain changed according to the rarefaction degree of the flow on the capsule.

The computational domain around the capsule is divided into an arbitrary number of regions, which are subdivided into computational cells. The cell provides a convenient reference for the sampling of the macroscopic gas properties. In addition, the cells are further subdivided into subcells. The subcell provides a reference for the collision process. The collision partners are selected from the same subcell in order to establish the collision rate. In the present investigation, it was defined two subcells/cell in each coordinate direction. As a result, the physical space network is used to facilitate the choice of molecules for collisions as well as for the sampling of the macroscopic flow properties, such as temperature, pressure, density, etc.

According to Fig. 2(b), side I is defined by the capsule surface. Reflection with incomplete surface accommodation is the condition applied to this side. Side II is a plane of symmetry, where all flow gradients normal to the plane are zero. At the molecular level, this plane is equivalent to a specular reflecting boundary. Side III is the freestream side through which simulated molecules enter and exit. Finally, the flow at the downstream outflow boundary, side IV, is predominantly supersonic and vacuum condition was assumed at this boundary (Bird, 1994). As a result, simulated molecules can only exit at this boundary. It is important to remark that, close to the wall, molecules may not be moving at supersonic speed. Consequently, in this subsonic region close to the wall, there is an interaction between the flow and the downstream boundary. Nevertheless, the extent of the upstream effect of this boundary condition can be determined by changing the length of the cone surface. In doing so, it was found that the upstream disturbance is approximately of $2\lambda_\infty$ for the altitudes investigated.

The numerical accuracy in DSMC method depends on the cell size chosen, on the time step as well as on the number of particles per computational cell. In the DSMC algorithm, the linear dimensions of the cells should be small in comparison with the length scale of the macroscopic flow gradients normal to streamwise directions. Therefore, the cell dimensions should be the order of or smaller than the local mean free path (Alexander $et\ al.$, 1998, 2000). Furthermore, the time step should be chosen to be sufficiently small in comparison with the local mean collision time (Garcia and Wagner, 2000; Hadjiconstantinou, 2000). In general, the total simulation time, discretized into time steps, is based on the physical time of the real flow. Finally, the number of simulated particles has to be large enough to make statistical correlations between particles insignificant.

These effects were investigated in order to determine the time steps, the number of cells, and the number of particles required to achieve grid independent solutions. Grid independence was tested by running the calculations with three different structured meshes – coarse, standard and fine – in each coordinate direction. The effect of altering the cell size in the ξ-direction was investigated for a coarse and fine grids with, respectively, 50% less and 100% more cells with respect to the standard grid only in the ξ-direction. In analogous fashion, an examination was made in the η-direction with a coarse and fine grids with, respectively, 50% less and 100% more cells with respect to the standard grid only in the η-direction. In addition, each grid was made up of non-uniform cell spacing in both directions. Moreover, point clustering was used close to capsule surface. Heat transfer, pressure and skin friction coefficients were selected in order to elucidate the requirements

posed for the grid sensitivity study. Distributions of these surface properties for the three grids were basically the same, an indication that the standard grid was rather insensitive to the range of cell spacing considered. A discussion of these effects on the aerodynamic surface properties is described in details by Santos (2012).

As part of the validation process, the axisymmetric version of this DSMC code was applied to a flat-ended circular cylinder in a rarefied hypersonic flow. Results for velocity, translational temperature, and rotational temperature distributions along the stagnation streamline were presented and compared with those obtained from another established DSMC code based in a code-to-code comparison. Again, this comparison is described in details by Santos (2012). Therefore, it will not be shown in this work.

7 COMPUTATIONAL RESULTS AND DISCUSSION

Incomplete surface accommodation effects on the primary properties acting on the SARA capsule are illustrated in this section by comparing simulated results for altitudes of 100, 95, 90, 85 and 80 km, which correspond to freestream Knudsen numbers of 0.4615, 0.1899, 0.0726, 0.0289, and 0.0115, respectively. Primary properties of particular interest are velocity, density, pressure, and temperature.

7.1 Velocity field

Tangential velocity profiles in the normal direction to the capsule surface is demonstrated in Figs. 3(a-c) for the diffuse reflection model as a function of the altitude for three stations along the capsule surface, defined by s/R of 0.4, 0.8, and 1.6, where s is the arc length along the surface measured from the stagnation point. The first two stations are located on the spherical nose, and the last one on the conical afterbody surface. In this set of plots, the tangential velocity u is normalized by the freestream velocity V_∞, and the height η in the off-body direction (η-direction in Fig. 2(a))

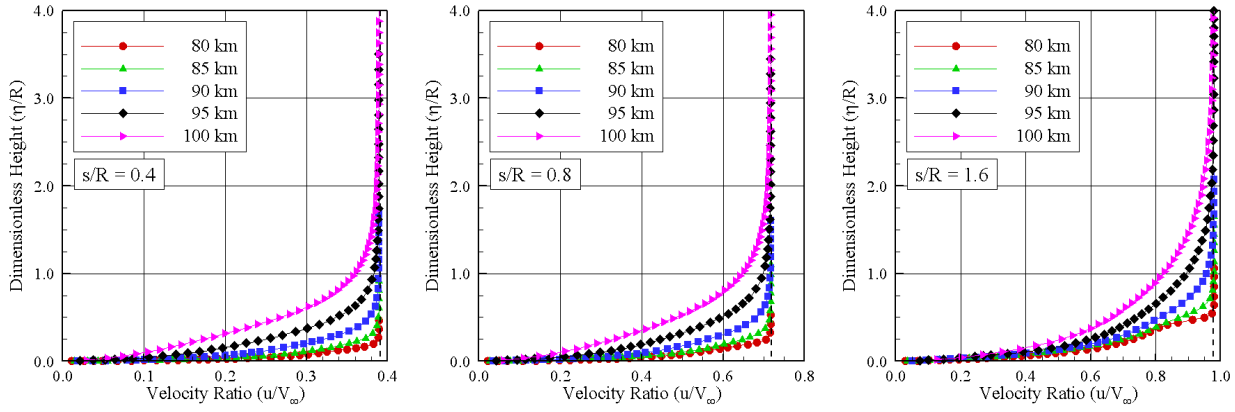

Figure 3: Tangential velocity (u/V_∞) profiles for the diffuse reflection model along the capsule surface for stations corresponding to s/R of (a) 0.4, (b) 0.8 and (c) 1.6.

is normalized by the capsule nose radius R. In addition, in order to emphasize points of interest, a different scale is used in the abscissa axis. It is important to note that V_∞ is slightly different for each altitude (see Table 1) and, therefore, the comparison is made in terms of ratio.

Interesting features can be drawn from this set of tangential velocity profiles. As the body slope decreases, i.e., as s/R increases, the tangential velocity u adjacent to the capsule surface increases. This is an expected behavior since the flow experiences an expansion as it moves downstream along the capsule surface. It is observed that the flow accelerates faster along the surface with the altitude rise. It should be noted that the tangential velocity u_∞, defined as $\eta \to \infty$, is represented by the dashed line and shown for each station. Because of the body curvature, u_∞(=$V_\infty \cos\theta$) varies as a function of the body slope.

Another interesting characteristic in these plots is the similarity of the velocity profiles along the capsule surface. This is an indication that the velocity profiles may be expressed in terms of functions that, in appropriate coordinates, may be independent of one of the coordinate directions. However, no attempts have been done to find such functions.

The effects of changing the normal α_n and tangential σ_t accommodation coefficients independently on the tangential velocity u in the capsule normal direction are depicted in Figs. 4 and 5 for altitudes of 100 km and 80 km, respectively, which correspond to Knudsen number Kn_∞ of 0.4615 and 0.0115, respectively. Tangential velocity profiles for others altitudes are intermediate to these profiles, therefore, they will not be shown. In this set of plots, for filled symbol curves, the tangential accommodation coefficient σ_t is varied from 0.25 to 1, while the normal accommodation coefficient α_n is held constant at 1. Also, for empty symbol curves, the normal accommodation coefficient α_n is varied from 0.25 to 1, while the tangential accommodation coefficient σ_t is held constant at 1. In addition, in an effort to emphasize points of interest, this set of plots presents data for three stations with a logarithm scale on the abscissa axis. Of great significance in this set of diagrams is the slip velocity. It is seen that slip velocity increases with decreasing the accommo-

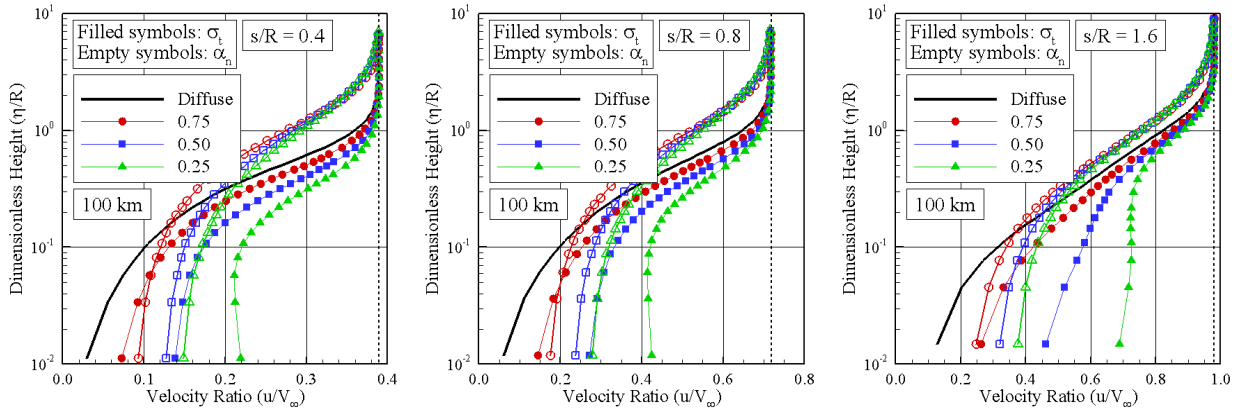

Figure 4: Tangential velocity (u/V_∞) profiles as a function of the normal and tangential accommodation coefficients for altitude of 100 km and for three stations along the capsule surface corresponding to s/R of (a) 0.4, (b) 0.8 and (c) 1.6.

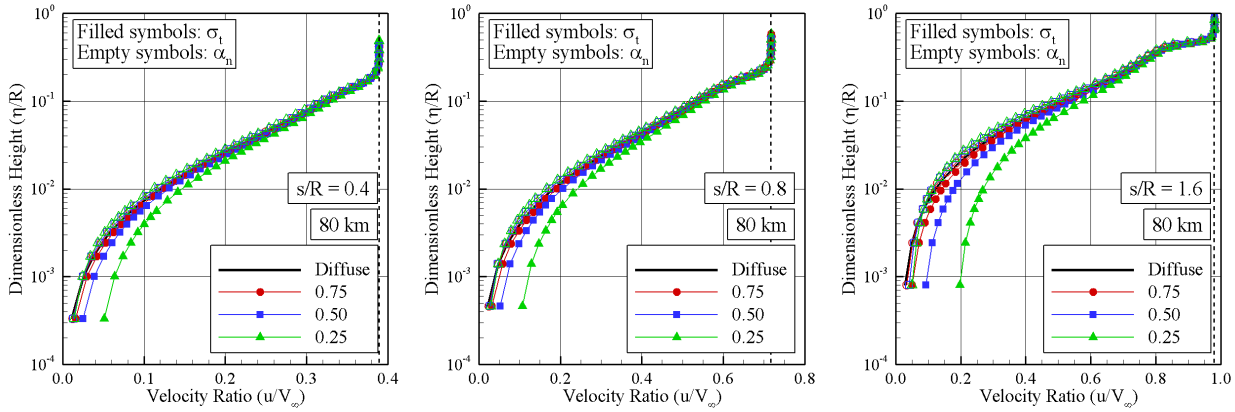

Figure 5: Tangential velocity (u/V_∞) profiles as a function of the normal and tangential accommodation coefficients for altitude of 80 km and for three stations along the capsule surface corresponding to s/R of (a) 0.4, (b) 0.8 and (c) 1.6.

dation coefficients. Nevertheless, the slip velocity effect is less pronounced with decreasing the altitude. As the altitude is reduced from 100 km to 80 km, the density increases around the capsule surface, as will be seen subsequently. Therefore, the molecular mean free path decreases, and the collision frequency increases adjacent to the capsule surface. As a result, the slip velocity is reduced. It should be noted in Figs. 4(a-c) that the tangential velocity reaches the freestream limit value u_∞, represented by the dashed line, close to the body surface for the station in the vicinity of the stagnation region. Because of the body curvature, u_∞ varies as a function of the body slope.

7.2 Density field

Density profiles by considering the diffuse reflection model along the capsule normal direction are depicted in Figs. 6(a-c) as a function of the altitude. This group of plots presents data at three stations that correspond to the dimensionless arc length s/R of 0.4, 0.8, and 1.6. According to these plots, dimensionless density stands for the density ρ normalized by the freestream density ρ_∞. It is clearly noticed that the density also experiences significant changes in the direction perpendicular to the wall as the flow moves downstream along the capsule surface. In the direction perpendicular to the wall, and for stations close to the stagnation region, the density is high adjacent to the wall and rapidly decreases inside a layer of thickness smaller than one nose radius R, where the density approaches the freestream value for the altitudes investigated. This characteristic is observed when the body surface is very much colder than the stagnation temperature of the oncoming gas, i.e., a characteristic of a cold-wall entry flow. As a result, the gas near the capsule surface tends to be much denser and cooler than the gas in the rest of the boundary layer. As a base of comparison, the ratio of wall temperature to stagnation temperature, T_w/T_o, is around 0.026. Conversely, for a station far from the stagnation region, s/R = 1.6, the density ratio is still maximum at the wall, it decreases in the off-body direction η and then it increases to a peak value inside the shock wave. Afterwards, the density decreases and reaches the freestream density value as $\eta/R \to \infty$.

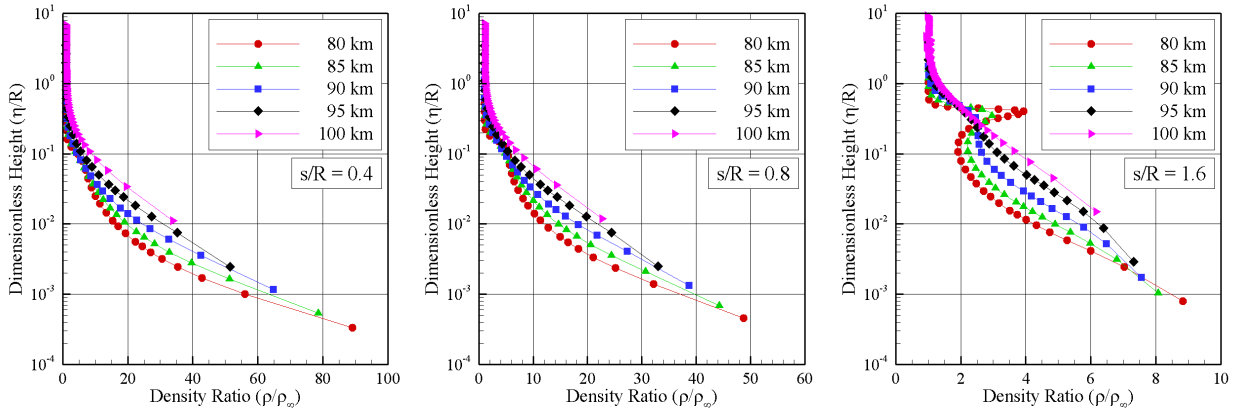

Figure 6: Density (ρ/ρ_∞) profiles for the diffuse reflection model along the capsule surface for stations corresponding to s/R of (a) 0.4, (b) 0.8 and (c) 1.6.

Still referring to Fig. 6, it is very encouraging to observe that density is affected by changes in the altitude, as would be expected. According to Fig. 6(a), which corresponds to the station s/R = 0.4, the density variation is in excess of one order of magnitude as compared to the freestream density for the altitude range investigated. In this region, close to the stagnation region, the compression combined with a relatively cool wall produces a maximum density ratio ρ/ρ_∞ that lies in the range from 40 to 90. In the following, because of the flow expansion along the afterbody surface, the density ratio adjacent to the capsule surface decreases dramatically to the range of 6 to 9 for the station s/R = 1.6.

Having a clear qualitative picture of the density behavior for the diffuse reflection model, the attention is turned to the effects of changing the normal α_n and tangential σ_t accommodation

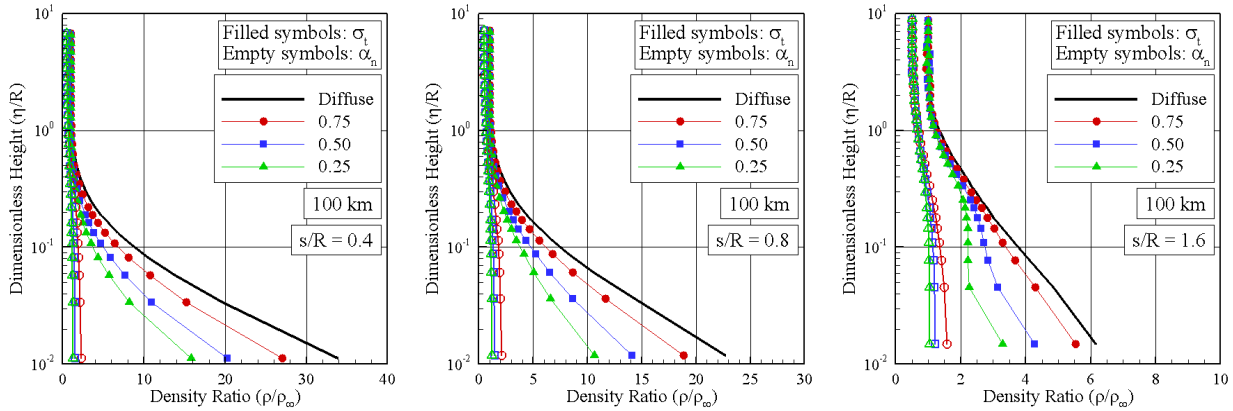

Figure 7: Density (ρ/ρ_∞) profiles as a function of the normal and tangential accommodation coefficients for altitude of 100 km and for three stations along the capsule surface corresponding to s/R of (a) 0.4, (b) 0.8 and (c) 1.6.

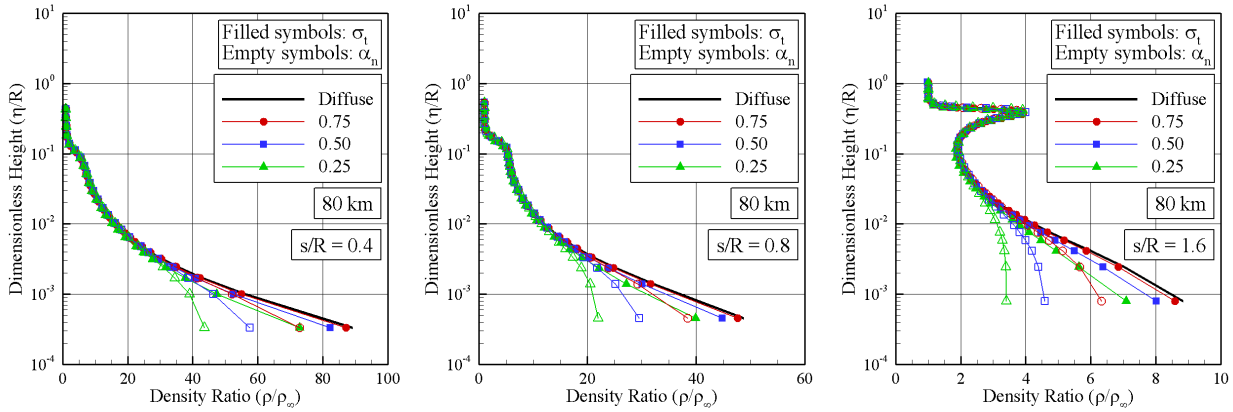

Figure 8: Density (ρ/ρ_∞) profiles as a function of the normal and tangential accommodation coefficients for altitude of 80 km and for three stations along the capsule surface corresponding to s/R of (a) 0.4, (b) 0.8 and (c) 1.6.

coefficients independently on density profiles. In this fashion, Figs. 7 and 8 illustrate these effects for altitudes of 100 km and 80 km, respectively, for the same three stations along the capsule surface. According to these plots, variations in α_n or σ_t seem to have approximately the same effect on density profiles for both altitudes in the sense that, as the accommodation coefficients decreases from 1 to 0.25, density ratio ρ/ρ_∞ decreases adjacent to the capsule surface for three stations shown. Nevertheless, the impact on density profiles is more pronounced as the normal accommodation coefficient α_n is reduced from 1 to 0.25.

It should be mentioned in this context that, for a cold-wall capsule, the diffusely reflected molecules remain in the vicinity of the surface longer and result in a density buidup near the capsule surface, as demonstrated by Figs. 6(a-c). Nevertheless, the CLL model provides a much more complex description of the velocity distribution of scattered molecules in the sense that, the overall mean velocity, temperature, and mean scattering angle are complex functions of the incoming velocity, wall temperature, and the normal α_n and tangential σ_t accommodation coefficients. For accommodation coefficients in the range $0 < \alpha_n(or\ \sigma_t) < 1$, the CLL model gives a somewhat higher average velocity of scattered molecules and a more continuous distribution of molecules scattered near the specular angle. Consequently, molecules do not remain near the surface and lower densities occur near the capsule surface, in contrast to those for the diffuse reflection model.

7.3 Pressure field

Local pressure p, expressed as a ratio to the freestream pressure p_∞, for the same three stations on the capsule surface is illustrated in Figs. 9(a-c) as a function of the altitude. It is apparent from these profiles that pressure is affected with decreasing altitude, or by decreasing the Knudsen number Kn_∞. For the station corresponding to s/R = 0.4, Fig. 9(a), the pressure is almost three orders of magnitude larger than the freestream pressure for an altitude of 80 km. In this region, at the vicinity of the stagnation point, the compression produces a maximum pressure that is around

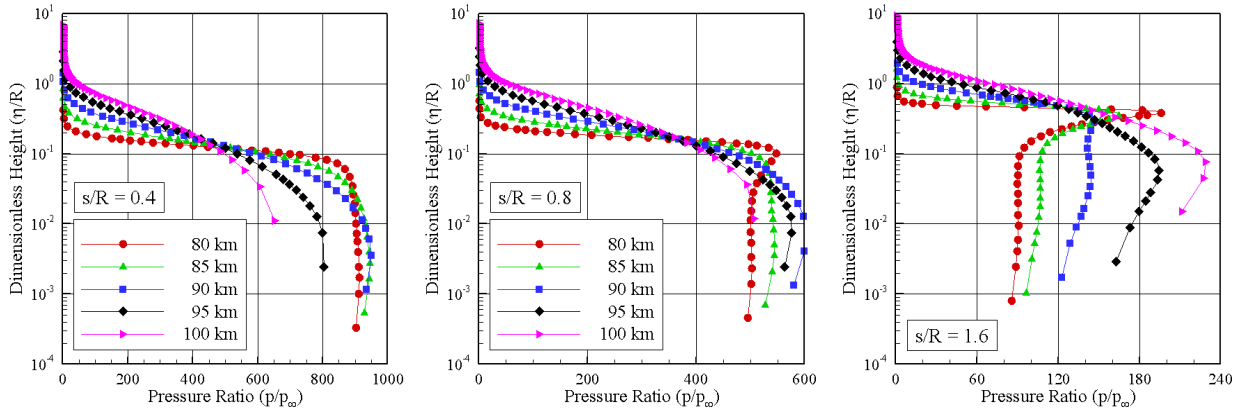

Figure 9: Pressure (p/p_∞) profiles for the diffuse reflection model along the capsule surface for stations corresponding to s/R of (a) 0.4, (b) 0.8 and (c) 1.6.

900 times the freestream pressure for an altitude of 80 km. Due to the flow expansion along the capsule surface, the pressure adjacent to the surface decreases significantly as s/R increases from 0.4 to 1.6. For the particular case of 80 km, the pressure ratio p/p_∞ decreases from 900 to around 80 for the station corresponding to s/R = 1.6, as shown in Fig. 9(c), a reduction of basically one order of magnitude.

The impact of changing the normal α_n and tangential σ_t accommodation coefficients independently on pressure p for three stations on the capsule surface are demonstrated in Figs. 10 and 11 for altitudes of 100 km and 80 km, respectively. It may be recognized from these plots that pressure ratio follows the same trend as that presented by density ratio in the sense that, as the accommo-

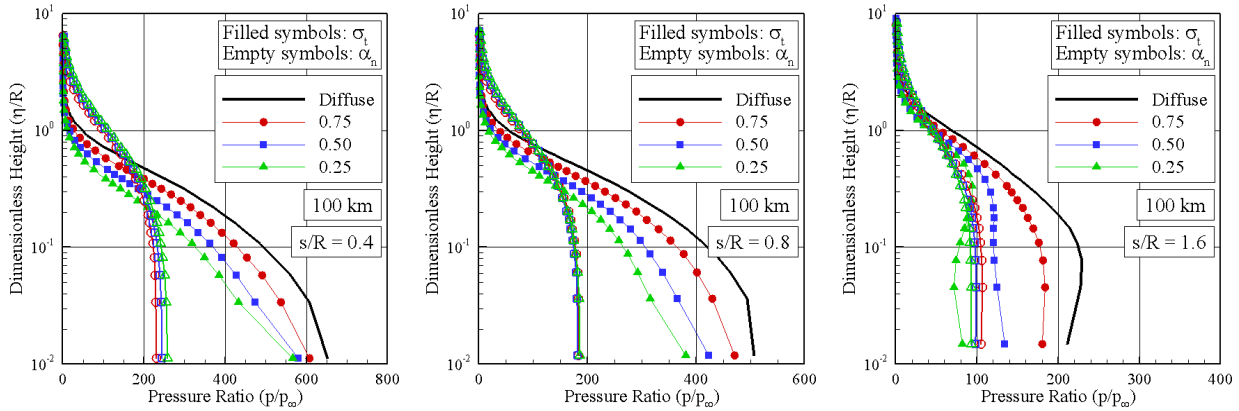

Figure 10: Pressure (p/p_∞) profiles as a function of the normal and tangential accommodation coefficients for altitude of 100 km and for three stations along the capsule surface corresponding to s/R of (a) 0.4, (b) 0.8 and (c) 1.6.

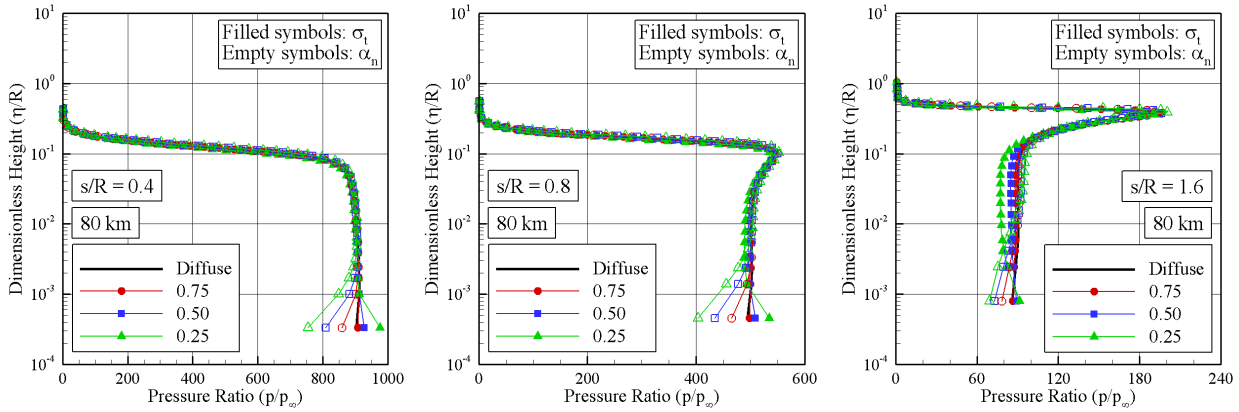

Figure 11: Pressure (p/p_∞) profiles as a function of the normal and tangential accommodation coefficients for altitude of 80 km and for three stations along the capsule surface corresponding to s/R of (a) 0.4, (b) 0.8 and (c) 1.6.

dation coefficients decreases from 1 to 0.25, pressure ratio p/p_∞ decreases adjacent to the capsule surface for three stations shown. Furthermore, similar to density ratio behavior, pressure ratio is more affected as the normal accommodation coefficient α_n is reduced from 1 to 0.25.

7.4 Temperature field

It is firmly established that a spacecraft entering into the atmosphere at hypersonic speed experiences two important features: (1) the strong shock wave that forms around the vehicle converts part of the kinetic energy of the freestream air molecules into thermal energy, the shock compression leads to strong molecular collisions. This thermal energy is partitioned into increasing the translational kinetic energy of the air molecules, and into exciting other molecular energy states such as rotation and vibration; (2) the low density of the atmosphere results in small molecular collision rates and, therefore, the thermal process may take place in local non-equilibrium conditions.

Thermal non-equilibrium occurs when the temperatures associated with translational, rotational, and vibrational modes of a polyatomic gas are different. In a thermodynamic non-equilibrium gas, an overall temperature is defined as the weighted mean of the translational and internal temperatures (Bird, 1994) as being,

$$T_{OV} = \frac{\zeta_T T_T + \zeta_R T_R + \zeta_V T_V}{\zeta_T + \zeta_R + \zeta_V} \tag{5}$$

were ζ is the degree of freedom and subscript T, R and V stand for translation, rotation and vibration, respectively.

Kinetic temperature profiles by considering diffuse reflection model are displayed in Figs. 12(a-c) for altitudes of 100, 90 and 80 km, respectively. In this set of plots, kinetic temperature ratio stands for the translational temperature T_T, rotational temperature T_R, vibrational temperature T_V or overall temperature T_{OV} normalized by the freestream temperature T_∞. Also, filled and empty

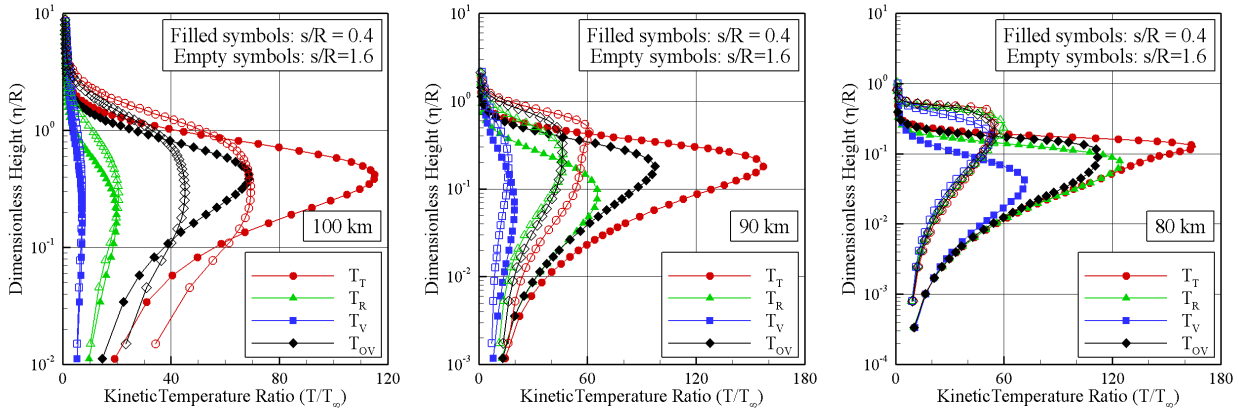

Figure 12: Kinetic temperature (T/T_∞) profiles for the diffuse reflection model as a function of the altitude for two stations along the capsule surface. (a) 100 km, (b) 90 km and (c) 80 km.

symbols correspond, respectively, to temperature distributions for two stations, s/R of 0.4 and 1.6, along the capsule surface. It is apparent from this set of plots that thermodynamic non-equilibrium occurs throughout the shock layer, as shown by the lack of equilibrium of the translational and internal kinetic temperatures.

According to Figs. 12(a-c), it is noticed that, in the undisturbed freestream far from the capsule surface, $\eta/R \rightarrow \infty$, the translational, rotational and vibrational temperatures have the same value and are equal to the thermodynamic temperature. Approaching the capsule surface, for instance, $\eta/R \approx 0.2$ for altitudes of 90 km, the translational kinetic temperature rises to well above the rotational and vibrational temperatures, and reaches a maximum value that is a function of the altitude. The translational kinetic temperature rise results from the essentially bimodal velocity distribution: the molecular sample consisting of mostly undisturbed freestream molecules with the molecules that have been affected by the shock and reflected from the capsule surface. In this manner, the translational kinetic temperature rise is a consequence of the large velocity separation between these two classes of molecules. In addition, since a large number of collisions is needed to excite the vibrational mode of the molecules from the ground state to the upper state, the vibrational temperature is seen to increase much more slowly than rotational temperature.

Still further toward the capsule surface, $\eta/R \approx 0$, the translational and kinetic temperatures decrease, and reach values on the wall that are above the wall temperature $T_W(\approx 4T_\infty)$, for altitude of 100 km, resulting in a temperature jump as defined in continuum formulation. Nevertheless, for altitudes of 90 km and 80 km, the difference between translational temperature and internal temperatures drastically decreases, and temperatures basically approach the wall temperature, indicating that the thermodynamic equilibrium is roughly achieved in this region. The reason for that comes from the fact that density dramatically increases adjacent to the capsule surface as the altitude decreases from 100 km to 80 km (see Fig. 6). Consequently, the molecular collision rate increases adjacent to the capsule surface.

In order to bring out the essential features of the incomplete accommodation on the capsule

surface, the effects of changing the normal α_n and tangential σ_t accommodation coefficients independently on translational temperature are displayed in Figs. 13 and 14 for altitudes of 100 km and 80 km, respectively, in the normal direction at stations s/R of 0.4, 0.8, and 1.6. According to these plots, it is clearly noticed that changes on α_n or on σ_t are more significant on translational temperature for altitude of 100 km than those for 80 km. It is quite apparent that decreasing α_n from 1 to 0.25 resulted in a large temperature jump at the capsule surface for the case of 100 km of altitude, as compared to that for the diffuse reflection model, shown in Fig. 12(a). This is explained by the fact that density decreases adjacent to the capsule surface by a reduction on α_n or on σ_t. As a result, the molecular collision rate is low adjacent to the capsule surface for the case of 100 km of altitude, which corresponds to a high Knudsen number, more precisely, Kn_∞ of 0.4615.

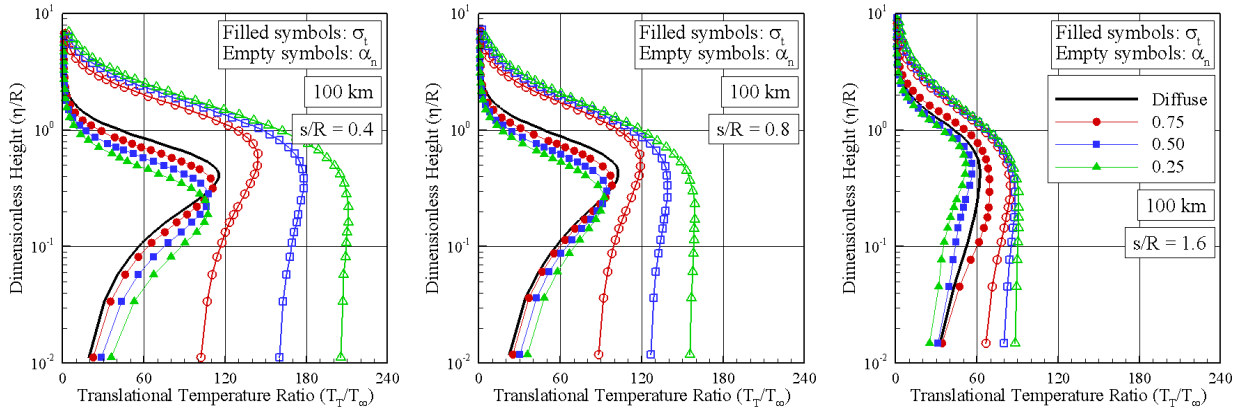

Figure 13: Translational temperature (T_T/T_∞) profiles as a function of the normal and tangential accommodation coefficients for altitude of 100 km and for three stations along the capsule surface corresponding to s/R of (a) 0.4, (b) 0.8 and (c) 1.6.

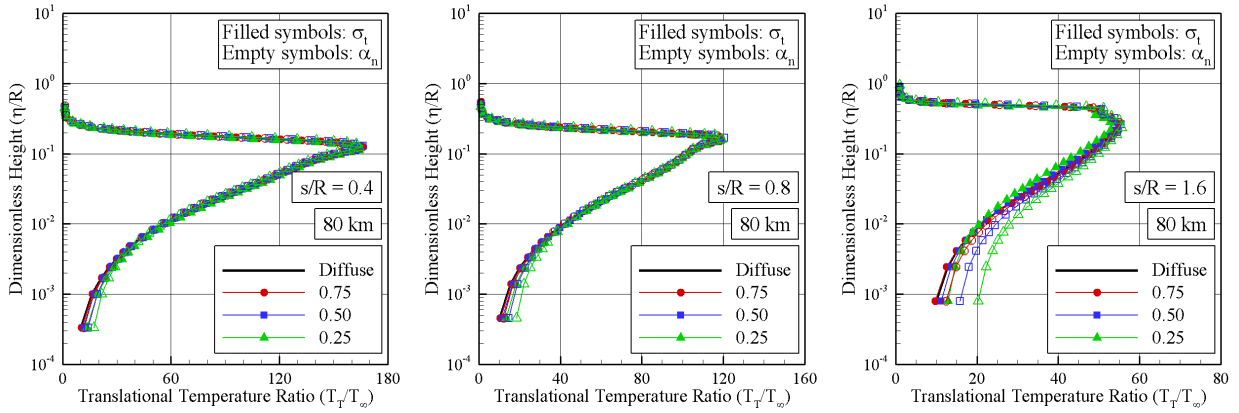

Figure 14: Translational temperature (T_T/T_∞) profiles as a function of the normal and tangential accommodation coefficients for altitude of 80 km and for three stations along the capsule surface corresponding to s/R of (a) 0.4, (b) 0.8 and (c) 1.6.

8 CONCLUDING REMARKS

In the current study, a rarefied hypersonic flow over the SARA capsule in its reentry trajectory have been performed by using the Direct Simulation Monte Carlo method. Simulations provided information concerning the behavior of the flowfield structure around the capsule by considering the impact of the gas-surface interactions.

Effects of incomplete surface accommodation on the velocity, density, pressure, and temperature for a representative range of parameters were investigated. The altitude varied from 100 km to 80 km, which corresponded to Knudsen numbers from 0.4615 to 0.0115, Reynolds numbers from 92 to 15249, and Mach numbers from 27 to 29. In addition, the normal and tangential accommodation coefficients varied independently from 0.25 to 1.0.

It was found that changes on the altitude as well as a reduction in the normal and tangential accommodation coefficients from 1.0 to 0.25 disturbed the flowfield around the capsule. The domain of influence decreased by decreasing the altitude. In addition, the domain of influence increased by decreasing the normal and tangential accommodation coefficients. Moreover, the extent of the flowfield disturbance around the capsule due to changes on the accommodation coefficients was significantly different for each one of the primary flow properties.

The present document has described an initial investigation of a high-altitude and low-density flow over the SARA capsule. Although this investigation has taken into account a representative range of altitudes, improvements are still desirable to a realistic capsule design. Since no database exist for such a design and since no appropriate flight data are available at such high entry velocities and conditions, the use of computational methods becomes essential.

ACKNOWLEDGEMENTS

The author would like to thank the financial support provided by CNPq (Conselho Nacional de Desenvolvimento Científico e Tecnológico) under Grant No. 312094/2009-4.

REFERENCES

Alexander, F. J., Garcia, A. L., & Alder, B. J., 1998. Cell size dependence of transport coefficient in stochastic particle algorithms. *Physics of Fluids*, vol. 10, n. 6, pp. 1540–1542.

Alexander, F. J., Garcia, A. L., & Alder, B. J., 2000. Erratum: Cell size dependence of transport coefficient in stochastic particle algorithms. *Physics of Fluids*, vol. 12, n. 3, pp. 731–731.

Bird, G. A., 1981. Monte Carlo simulation in an engineering context. In Fisher, S. S., ed., *Progress in Astronautics and Aeronautics: Rarefied gas Dynamics*, vol. 74, part I, AIAA New York, pp. 239–255.

Bird, G. A., 1989. Perception of numerical method in rarefied gasdynamics. In Muntz, E. P., Weaver, D. P., and Capbell, D. H., eds., *Rarefied Gas Dynamics: Theoretical and Computational Techniques*, vol. 118, Progress in Astronautics and Aeronautics, AIAA, New York, pp. 374–395.

Bird, G. A., 1994. *Molecular gas dynamics and the direct simulation of gas flows*. Oxford University Press.

Borgnakke, C. & Larsen, P. S., 1975. Statistical collision model for Monte Carlo simulation of polyatomic gas mixture. *Journal of Computational Physics*, vol. 18, n. 4, pp. 405–420.

Cercignani, C., 1972. Scarrering kernels for gas-surface interactions. *Transport Theory and Statistical Physics*, vol. 2, n. 1, pp. 27–53.

Cercignani, C. & Lampis, M., 1971. Kinetic models for gas-surface interactions. *Transport Theory and Statistical Physics*, vol. 1, n. 2, pp. 101–114.

Garcia, A. L., & Wagner, W., 2000. Time step truncation error in direct simulation Monte Carlo. *Physics of Fluids*, vol. 12, n. 10, pp. 2621–2633.

Hadjiconstantinou, N. G., 2000. Analysis of discretization in the direct simulation Monte Carlo. *Physics of Fluids*, vol. 12, n. 10, pp. 2634–2638.

Hedahl, M. O. & Wilmoth, R. G., 1995. Comparison of the Maxwell and the CLL gas-surface interacion models using DSMC. NASA TM-110205.

Kozak, D. V., & Sharipov, F., 2012. Aerothermodynamics of satellite during atmospheric reentry for the whole range of gas rarefaction: influence of inelastic intermolecular collisions. *Brazilian Journal of Physics*, vol. 42, pp. 192–206.

Lord, R. G., 1991. Application of the Cercignani-Lampis scattering kernel to direct simulation Monte Carlo method. In *Proceedings of the 17th International Symposium on Rarefied Gas Dynamics*, edited by A. E. Beylich, pp. 1427-1433, 8–14 July, Aachen, Germany.

Maxwell, J. C., 1879. On stresses in rarefied gases arising from inequalities of temperature. *Philosophical Transactions of the Royal Society of London*, vol. 170, Pt. 1, pp. 231–256, reprinted in The Scientific Papers of J. C. Maxwell, Dover, New York, 1965.

Pimentel, C. A. R., Azevedo, J. L. F., Korzenowski, H., & Mantelli, M. B. H., 2005. Chemical equilibrium inviscid flow over SARA re-entry vehicle. In *Proceedings of the 43rd AIAA Aerospace Sciences Meeting and Exhibit*, AIAA, Paper 2005–0390, 10–13 January, Reno, NV.

Santos, W. F. N., 2012. Aerothermodynamic analysis of a reentry Brazilian satellite. *Brazilian Journal of Physics*, vol. 42, pp. 373–390.

Sharipov, F., 2003. Hypersonic flow of rarefied gas near the Brazilian satellite during its reentry into atmosphere. *Brazilian Journal of Physics*, vol. 33, n. 2, pp. 398–405.

Tchuen, G., Burtschell, Y., & Zeitoun, D. E., 2005. Numerical prediction of nonequilibrium hypersonic flow around Brazilian satellite SARA. *Brazilian Journal of Physics*, vol. 35, n. 1, pp. 148–156.

Toro, P. G. P., Minucci, M. A. S., Ramos, A. G., Chanes Jr., J. B., Pereira, A. L., Korzenowski, H., Nagamatsu, H. T., & Myrabo, L. N., 2001. Experimental investigation of blunt body at Mach 8. In *Proceedings of the 39th AIAA Aerospace Sciences Meeting and Exhibit*, AIAA, Paper 2001–0644, 8–11 January, Reno, NV.

Toro, P. G. P., Minucci, M. A. S., Chanes Jr., J. B., & Ramos, A. G., 2004. Experimental hypersonic investigation over the micro-satellite SARA. In *Proceedings of the 10th Brazilian Congress of Thermal Sciences and Engineering*, Rio de Janeiro, RJ, Brazil.

Woronowicz, M. S. & Rault, D. F. G., 1994. Cercignani-Lampis-Lord gas-surface interacion model: comparisons between theory and simulation. *Journal of Spacecraft and Rockets*, vol. 31, n. 3, pp. 532–534.